JPRS 77556

10 March 1981

China Report

SCIENCE AND TECHNOLOGY

No. 86

FBIS FOREIGN BROADCAST INFORMATION SERVICE

NOTE

JPRS publications contain information primarily from foreign newspapers, periodicals and books, but also from news agency transmissions and broadcasts. Materials from foreign-language sources are translated; those from English-language sources are transcribed or reprinted, with the original phrasing and other characteristics retained.

Headlines, editorial reports, and material enclosed in brackets [] are supplied by JPRS. Processing indicators such as [Text] or [Excerpt] in the first line of each item, or following the last line of a brief, indicate how the original information was processed. Where no processing indicator is given, the information was summarized or extracted.

Unfamiliar names rendered phonetically or transliterated are enclosed in parentheses. Words or names preceded by a question mark and enclosed in parentheses were not clear in the original but have been supplied as appropriate in context. Other unattributed parenthetical notes within the body of an item originate with the source. Times within items are as given by source.

The contents of this publication in no way represent the policies, views or attitudes of the U.S. Government.

PROCUREMENT OF PUBLICATIONS

JPRS publications may be ordered from the National Technical Information Service, Springfield, Virginia 22161. In ordering, it is recommended that the JPRS number, title, date and author, if applicable, of publication be cited.

Current JPRS publications are announced in Government Reports Announcements issued semi-monthly by the National Technical Information Service, and are listed in the Monthly Catalog of U.S. Government Publications issued by the Superintendent of Documents, U.S. Government Printing Office, Washington, D.C. 20402.

Indexes to this report (by keyword, author, personal names, title and series) are available from Bell & Howell, Old Mansfield Road, Wooster, Ohio 44691.

Correspondence pertaining to matters other than procurement may be addressed to Joint Publications Research Service, 1000 North Glebe Road, Arlington, Virginia 22201.

JPRS 77556

10 March 1981

CHINA REPORT

SCIENCE AND TECHNOLOGY

No. 86

CONTENTS

PHYSICAL SCIENCES

HIGH EFFICIENCY PACKINGS IN ISOTOPE SEPARATING COLUMN STUDIED

Shanghai HE JISHU [NUCLEAR TECHNIQUES] in Chinese No 6, 1980 pp 18-22

[Article by Yang Guohua [2799 0948 5478], Lu Weiguo [7120 4850 0948], Wang Rong [3076 5816] and Ceng Quanxing [2582 2938 5281] of Shanghai Research Institute of Chemical Industry: "The Performances of Three High Efficiency Packings Used in Isotope Separating Column"]

[Text] Abstract

This article was received on 19 June 1979. The major performances of three high efficiency packings were studied in the enrichment of ^{13}C using CO_2/ di-n-butylamine (DNBA)/ triethylamine (TEA) system. These packings consisted of 2x2mm Dixon rings (phosphor bronze gauze, 100 mesh), 1.5x1.5x0.12mm triangular-section spirals (stainless steel wire ϕ 0.12mm) and 1.6x0.6x1.5x0.12mm rectangular-section spirals (i.e., Helipak packings, stainless steel wire ϕ 0.12mm). The results showed that the spiral packings are very suitable for chemical exchange processes of isotope separation which require theoretically a large number of plates.

As is well known, isotopes have identical electronic structure outside the nucleus and differ only in the number of neutrons inside the nucleus. Since they are very similar in physical and chemical properties, they are difficult to separate. To achieve a high degree of separation it requires theoretically a large number of plates and separating stages. For example, 90 percent concentration ^{13}C requires more than 1,000 theoretical plates.

The chemical exchange method of vapor-liquid countercurrent contacting is a major technique in stable isotope enrichment. High efficiency packing columns are generally used in this method; therefore, the crucial factor of the packing suitable for isotope separation is that the theoretical number of plates per meter $\bar{N}$ should be as large as possible. According to the theory of Cohen[1], $\bar{N}$ of a 1 meter packing is directly proportional to the inter-phase effective surface area a_e

$$\bar{N} = Ka./L \qquad (1)$$

where K is the transport coefficient, dependent upon the physical property and the flow of vapor and liquid; a_e is the vapor-liquid contact surface area per unit volume of packing, also known as the effective ratio surface; and L is the liquid flow density. As can be seen from Eq.(1), whether or not a packing has high efficiency for isotope separation is determined mainly by a_e. For a large a_e, a packing must first have a large geometric surface area a and the wetting condition of the packing is described by

$$a_e = \varphi a, \quad (\varphi < 1) \qquad (2)$$

For complete wetting, $\varphi = 1$. So the necessary condition for high efficiency is a large a and the sufficient condition is a large φ. φ depends on the system, the material of the packing, the surface condition of the packing and the distribution of vapor and liquid in the column.

Akonov et al[2] have made detailed evaluation of packings used in isotope separating column but provided no direct comparison to experimental data. In this paper we have made direct experimental comparison of the performances of three high efficiency packings used in the ^{13}C enrichment in a CO_2/ di-n-butylamine (DNBA)/ triethylamine (TEA) vapor-liquid chemical exchange system to select the most suitable packing. The three packings used are 2x2mm Dixon rings, 1.5x1.5x0.12mm triangular spirals and 1.6x0.6x1.5x0.12mm rectangular spirals.

In the process of isotope separation pressure drop and holdup are admittedly important factors; however, since the vapor liquid ratio in an isotope chemical exchange process is usually smaller than that in a distillation process, the pressure drop is usually not large. In addition, the ease of packing fabrication is also an important factor in the selection consideration.

Experiment

Figure 1 shows the experimental flow diagram. Exchange colume is made of glass and has an inner diameter of 15mm. The height of the packing is 4m.

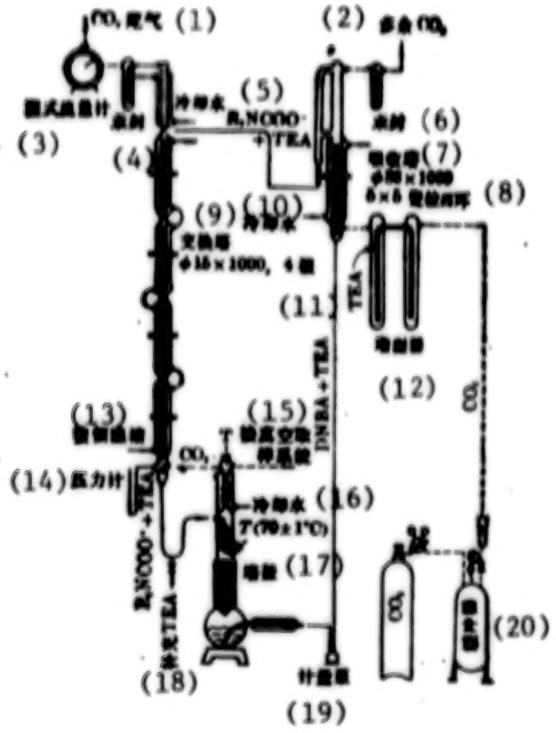

Fig. 1 Experimental Flow Diagram
(1.5M DNBA-TEA/CO_2 system)

Key:

1. Tail gas
2. Excess CO_2
3. Wet flow meter
4. Mercury seal
5. Cooling water
6. Mercury seal
7. Absorption column
8. Ceramic ring
9. Exchange column
10. Cooling water
11. Four stages
12. Humidifier
13. To constant temperature bath
14. Pressure gauge
15. To vacuum sampling system
16. Cooling water
17. Boiler
18. Supplemental TEA
19. Metering pump
20. Buffer tank

In the absorption column 1.5M solutions of DNBA and TEA absorb CO_2 and form carbamate of DNBA:

$$R_2NH + CO_2 \longrightarrow R_2NCOO^- + \Delta H \qquad (3)$$

where R is an alkyl group. R_2NCOO^- flows downward through the exchange column and reaches the boiler where it is heated and decomposes into CO_2 and solutions of DNBA and TEA:

$$R_2NCOO^- \xrightleftharpoons{\Delta} R_2NH+CO_2\uparrow \qquad (4)$$

(At 105 ~ 107°C, boiling decomposition is complete and heat conduction chromatographic analysis of residual CO_2 shows that the content is less than 20 ppm.) The DNBA and TEA solutions are then transported by a metering pump to the bottom of the absorption column where they are reused. CO_2 enters the bottom of the exchange column and makes countercurrent contact with carbamate as it flows upward and leads to the following isotope chemical exchange:

$$R_2N^{12}COO^- + {}^{13}CO_2 \rightleftharpoons R_2N^{13}COO^- + {}^{12}CO_2 \qquad (5)$$

$$a = 1.01(25 \sim 28°C)$$

Concentrated ^{13}C flows to the bottom of the column. The excess CO_2 containing reduced abundance of ^{13}C is then exhausted outside the laboratory. The accuracy of the metering pump is $\pm 1\%$. CO_2 sample gas flows from the cylinder through a buffer, a rotary flow meter and a humidifier to the bottom of the absorption column. The CO_2 flow rate is maintained slightly larger than that required for the chemical reaction to ensure saturation in the absorption. (Excess CO_2 bubbles escape from the liquid surface at the top of the absorption column.) The inner diameter of the absorption column is 36 mm, the length is 1 m and it is fitted with 5x5 ceramic ring. The humidifier has two tubes, one contains TEA and the other is empty. The purpose of the humidifier is to maintain a TEA equilibrium in the system so that the amount of TEA depleted by tail gas (in the form of saturated vapor) is equal to that carried in by the sample gas and the amine concentration in the solution is maintained relatively constant. The function of the empty tube in the humidifier is to prevent TEA from entering the CO_2 intake line and the rotary flowmeter in case of a back pressure.

In order to determine the actual effective length of the exchange column, the absorption column used is of the concurrent type. Exchange column has four sections each with a 1 m packing. The jacket temperature is maintained at 28 ~ 30°C and the pressure at the top of the exchange column is kept at a constant 30 mm Hg. A flow meter is used in estimating the CO_2 absorption by the solution; measurement result shows that each gram molecule of DNBA absorbs 0.803 ~ 0.814 gram molecule of CO_2. This result is in agreement with $m/M = 0.8$ reported in Ref. (3).

All DNBA and TEA used in the experiment are of the chemical reagent grade and the CO_2 from the gas cylinder is at least 99 percent pure. During the entire experiment, all major parameters are kept within tolerance with automatic controlling devices. The concentration of DNBA in TEA solution is

measured with gas-liquid chromatography using 102 carrier + PEG (polyethylene glycol) + 5% KOH. The concentration of ^{13}C in CO_2 is determined using a model ATLAS-CH_4 mass spectrometer with a relative error less than 1 percent. The concentration, C, and the separation, S, are given below in terms of peak heights of mass 44 and mass 45:

$$C = \frac{\text{Peak height of mass 44}}{\text{Peak height of mass 44 + peak height of mass 45}} \quad (6)$$

$$S = \frac{\text{C of } CO_2 \text{ at bottom of column}}{\text{C of sample } CO_2} \quad (7)$$

Packing

Major parameters of the three packings are listed in Table 1. The ⊖ ring, also known as the Dixon ring, is rolled from 100 mesh phosphor bronze gauze. Triangular spirals are made by wrapping stiff stainless steel wire on a triangular conic tool. Elastic force keeps the spirals apart. Spirals assume random orientation and keep a certain distance in between. Rectangular spirals are made in a similar fashion except the tool is four squared, with a rectangular cross section. Although the equivalent dimensions of the latter two spiral packings are smaller than that of Dixon rings, they are easier to make. Dixon rings are washed in benzene and then the surface is treated with dilute hydrochloric acid (pH = 1). The surface of spiral packings is treated with 10 percent sulphuric acid after a rinse in benzene.

Table 1. Major Parameters of the Three Types of Packings

主要参数 (1) \ 填料名称 (2)	⊖ 环 (3) (Dixon)	三角形螺旋圈 (4)	矩形螺旋圈 (5) (Helipak)
材质 (6)	100 目磷青铜丝网 (7)	φ0.12mm不锈钢丝(有弹性) (8)	φ0.12mm 不锈钢丝(有弹性) (9)
几何尺寸 (10)	φ 2 mm 长 2mm (11)	正三角形，边长 1.5 mm 填料长 1.5 mm (12)	矩形长 1.6 mm 宽 0.6mm 填料长 1.5 mm (13)
(14) 每个填料几何表面积 (cm^2)	0.331	0.170	0.166
(15) 每cm^3填料个数 (最大装填)	105	300	306
(16) 最大堆填重量 (g/cm^3)	0.64	1.13	1.12
(17) 空隙率 (%)	92.7	85.5	85.6
(18) 比表面 a (cm^2/cm^3)	34.8	50.0	50.8

[Key to Table 1 on following page]

[Key to Table 1]

Key:

1. Major parameter
2. Type of packing
3. D xon ring
4. Triangular spiral
5. Rectangular spiral (Helipak)
6. Material
7. 100 mesh phosphor bronze gauze
8. 0.12mm stainless steel wire (springy)
9. 0.12mm stainless steel wire (springy)
10. Geometric dimensions
11. 2mm diameter, 2mm long
12. Right triangle, 1.5mm each side, packing spiral length is 1.5mm
13. Length of rectangle is 1.6mm, width is 0.6mm, packing spiral length is 1.5mm
14. Geometric surface area of packing (cm^2)
15. Number of packing per cm^3 (max. packing)
16. Maximum weight (g/cm^3)
17. Porosity (%)
18. Effective ratio surface (cm^2/cm^3)

Results and Discussions

1. Theoretical plate number per meter, $\bar{N}$

Under the condition of no product withdrawal, a simple relationship exists between the theoretical plate number N and the separation factor S

$$N = \ln S / \ln \alpha \qquad (8)$$

where α is the coefficient of separation. Theoretical plate number per meter, $\bar{N}$, of the packing is then given by

$$\bar{N} = N/Z \qquad (9)$$

in which Z is the height of the packing in meters.

From Eq.(1) one can see that $\bar{N}$ decreases with increasing L but the relationship is not simply inversely proportional because K_{a_e} also depends on L. Generally speaking $\bar{N}$ is a maximum when L is optimum and the wetting condition and vapor liquid contact are most ideal. Too large an L does not improve the wetting condition any further but reduces $\bar{N}$ because the increased liquid film thickness is detrimental to diffusion. On the other hand, $\bar{N}$ also decreases when L is too small due to insufficient wetting. Table II gives the experimental results for the three types of packings. $\bar{N}$ is found to vary with the flow rate and the separation factor in these experiments.

Table II. Experimental Results of the Three Packings

(1) 填料名称	流量(2)		(3) 分离度	每米理论板数	当量理论板高度	分离能力(6)	每米阻力降	持留量 (8)
	L	G	S	$\overline{N}$ (4)	$HETP$ (5)	$F=G/(HETP)$	ΔP (7)	θ
	ml/cm² · min	m atom C /cm² · min		块/m (9)	cm	m atom C /cm² · min	mmH₂O柱 /m (10)	ml/cm²
2×2θ 环 (DNBA 浓度 2M) (11)	0.81	1.30	2.58	23.7	4.2	0.294	6	
	1.62	2.59	1.78	14.5	6.9	0.374	8	
	3.46	5.54	1.86	15.8	6.4	0.872	12	
1.5×1.5×0.12 三角形螺旋圈 (12)	1.06	1.27	4.91	40	2.5	0.508	5	0.119
	2.12	2.55	5.13	41	2.4	1.043	14	0.125
	4.53	5.44	4.54	38	2.6	2.07	18	0.197
	5.67	6.80	3.58	32	3.1	2.17	22	0.228
	6.85	8.21	2.72	25	4.0	2.07	27	0.247
1.6×0.6×1.5 ×0.12矩形 螺旋圈 (13)	1.06	1.27	5.13	41	2.4	0.520	5	0.112
	4.53	5.44	4.54	38	2.6	2.07	17	0.200
	6.85	8.21	2.84	26	3.8	2.16	25	0.252

注：(1) α=1.01 m/M=0.8 mol CO_2/mol DNBA (2) 原料 CO_2 中 ^{13}C 天然丰度=1.1% (3)流量和分离能力单位中的 m atom C 为毫克原子碳。

Note (a) α = 1.01, m/M = 0.8 mol CO_2/mol DNBA
(b) Natural abundance of ^{13}C in sample CO_2 = 1.1%
(c) The factors 'm atom C' in the units of flow rate and separation power represent 'milligram atomic carbon'

Key:
1. Type of packing
2. Flow rate
3. Separation
4. Theoretical plate number per meter
5. Height Equivalent of Theoretical Plate (HETP)
6. Separation power
7. Pressure drop per meter
8. Holdup
9. Plate number per meter
10. mm H_2O column/m
11. 2x2mm Dixon ring (DNBA concentration = 2M)
12. Triangular spirals
13. Rectangular spirals

Figure 2 shows that the major characteristics of the two spiral packings are quite similar. Good efficiencies are achieved in the range of L = 1～3.5 ml/cm^2 and the variation of efficiency is relatively small. The spirals are found to have good elasticity and are better than Dixon rings as packings in chemical exchange isotope separation.

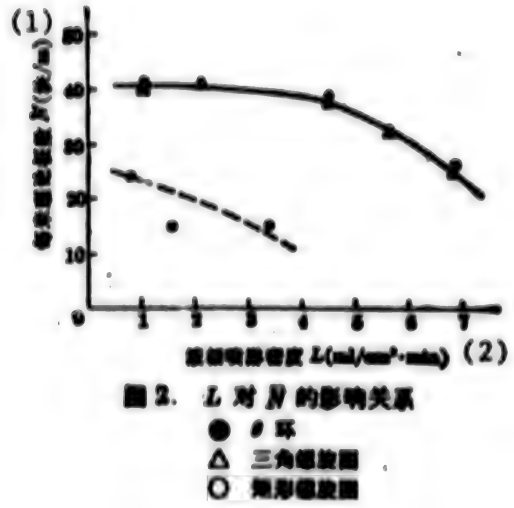

图 2. L 对 $\bar{N}$ 的影响关系

● θ 环

△ 三角螺旋圈

○ 矩形螺旋圈

Fig. 2 $\bar{N}$ as a function of L

● Dixon ring △ Triangular spiral ○ Rectangular spiral

Key:

1. Theoretical plate number per meter
2. Liquid spray density [flow rate] L

2. Separation power F

Although $\bar{N}$ is an important factor of the packing, it can only reflect the required column height for a given separation task, that is, the larger the $\bar{N}$, the smaller the required column height Z. Certain packings, despite their lower efficiency, can operate under a greater flow rate. In such cases one would rather increase the column height and decrease the column radius and volume in exchange for a lower demand on the amount of packing. In the meantime a smaller column radius means a correspondingly smaller amplification effect and certain advantages can be gained in improving the efficiency. For these reasons the separation power F, defined as:

$$F = \bar{N}G/100 = G/HETP, \qquad (10)$$

is also used in the evaluation of the packing efficiency. The physical meaning of F is the separating ability of a unit theoretical section volume of packing. G in Eq.(10) is the gas flow per unit area in a unit time. The unit of G is m atom C/cm^2· min.

Figure 3 shows the dependence of F on L. For industrial flow rates the two spiral packings have greater separating ability. They will therefore lead to more economical usage of packings and reduced capital investments.

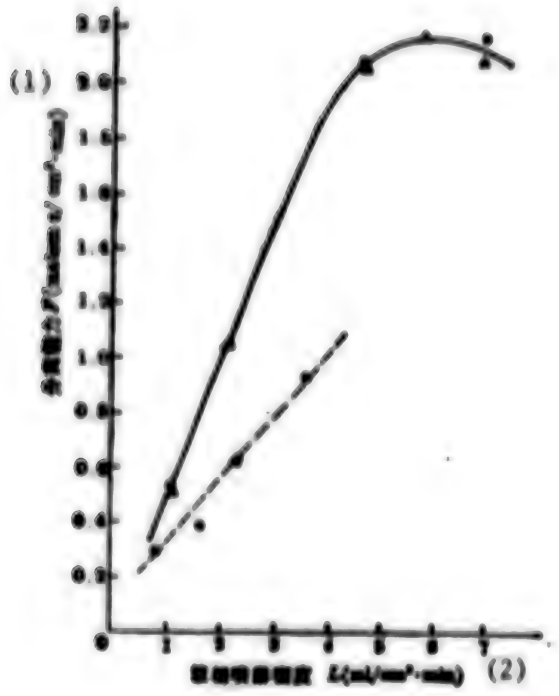

Fig. 3 L dependence of P

● Dixon ring △ Triangular spiral ○ Rectangular spiral

Key:

1. Separation power
2. Liquid phase flow rate

3. Pressure drop ΔP and holdup Ω

Since the vapor and liquid volumes in our experimental system are relatively small (as compared to distillation process), the pressure drop ΔP is also small. This is very favorable for high concentration isotope enrichment processes where series of high columns are required. Figure 4 shows the L dependence of the pressure drop per meter in the three types of packings. Within the range of the experiment the relationship is linear.

Figure 5 shows the L dependence of holdup Ω in a unit volume of packing. It shows that, within the experimental range, Ω is a linear function of L. In the range of L = 1 $\sim$ 4 ml/cm^2·min. Ω is less than 20 percent of the packing volume. Such moderate amounts of holdup are suitable for isotope separation process.

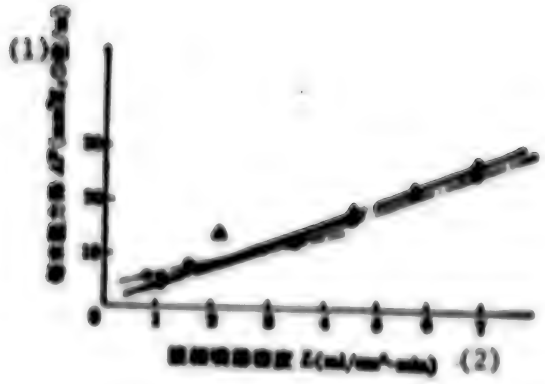

Fig. 4 L dependence of ΔP

● Dixon △ Triangular spiral ○ Rectangular spiral

Key:
1. Pressure drop per meter (mm H_2O column/ m)
2. Liquid phase flow rate

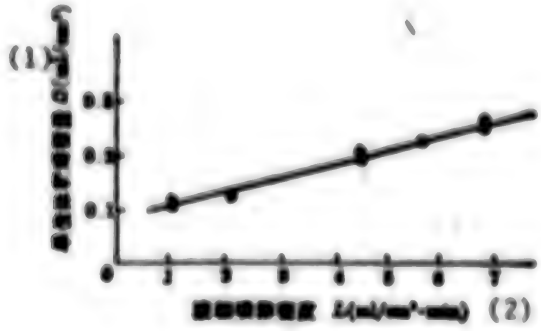

Fig. 5 Ω as a function of L

● Triangular spiral ○ Rectangular spiral

Key:
1. Unit volume holdup
2. Liquid phase flow rate

4. Estimate of errors

The main components of error, $\Delta \bar{N}$, in the measurements of $\bar{N}$ is the error ΔC in the analysis of ^{13}C concentration. The relative analysis error of the natural abundance is twice the $\Delta C/C$ of the sample. For constant α and Z, the dependence of $\Delta \bar{N}$ and $\Delta \bar{N}/\bar{N}$ on $\Delta C/C$ can be derived from Eqs.(7), (8) and (9):

$$\Delta \bar{N} < 3 \frac{\Delta c}{c} / 2\mathcal{E} \quad \mathcal{E} = \frac{\alpha - 1}{\alpha} \tag{11}$$

$$\Delta \bar{N} < 3 \frac{\Delta c}{c} / \ln\beta \tag{12}$$

It is evident that the greater the values of Z and $\mathcal{E}$, the smaller the error in $\bar{N}$. Minor contributions to the error $\Delta \bar{N}$ are due to error in flow rate, ΔL, and due to the fluctuation of temperature. The combined result is $\Delta N < 2$ plates/m, $\Delta N / \bar{N} = 5 \sim 8\%$.

Acknowledgements

This work has benefited from the excellent assistance of Zhou Yuncheng [0719 0061 4453] and Sun Shiquan [1327 2514 5425] in isotope analysis. We appreciate their contribution.

References

(1) K. Cohen, "The Theory of Isotope Separation," McGraw-Hill, New York, 1951.

(2) Yu. R. Akonov et al, ATOMIC ENERGY, 17, 5, 384 (1964)

(3) M. R. Ghate and T. I. Taylor, USAEC COO-3263-3, 1973.

(4) M. R. Ghate and T. I. Taylor, Separ. Sci., 10, 5, 547 (1975).

(5) Ye. D. Oziashvili et al, Stable Isotopes in the Life Sciences, IAEA, Vienna, 1977, p 29.

9698
CSO: 4008

'JOURNAL OF CHINESE SOCIETY OF ASTRONAUTICS' FOUNDED

Beijing YUHANG XUEBAO [JOURNAL OF THE CHINESE SOCIETY OF ASTRONAUTICS] in Chinese No 1, 1980 pp I, II

[Article by Zian Xuesen [6929 1331 2773], Honorary director of the Chinese Society of Astronautics: "Congratulatory Remarks On the Issuance of Yuhang XUEBAO [JOURNAL OF THE CHINESE SOCIETY OF ASTRONAUTICS]

[Text] I think the Space Navigation Society has a very bright future.

The first phase of space navigation is space flight, by which is meant the movement by man in a sphere of perhaps 1 billion kilometers within the solar system. I believe that space flight technology is one part of the technological revolution that Chairman Mao defined, and that it is a singular technological revolution on a par with the steam engine, electric power, atomic energy, and electronic calculators. The impact of spaceflight technology on the development of social productivity and on national construction has just begun to become apparent. We can foresee that the role of spaceflight technology will positively be no less than the space navigation with which everyone is familiar.

Spaceflight technology also provides us the possibility of vaulting away from the earth to traverse the atmosphere and to survey the universe. It has greatly expanded our horizons and removed the scales from our eyes. During the past several years, the development of high energy astronomy has profoundly increased our knowledge of the universe, and it will both enrich and deepen the dialectic materialist view of nature, thereby expanding the philosophy of Marxism.

But this is but the first stage. The second stage of space navigation is to escape from the solar system to interstellar space, to travel the Milky Way galaxy, or even to greater limits of the universe! The requirements for space navigation technology are higher than for spaceflight technology. A speed of movement of several score kilometers per second is not enough; only a speed of movement close to the speed of light will do. Moreover, even though the interval of time aboard the flight vehicle will not be very long, the wait back home on earth for the planned completion of a trip into the universe may be as long as up to more than a decade, several hundred years, or several thousand years! This is something that very obviously neither the science and technology of today nor the science and technology of tomorrow can solve. To complete the

course of the second stage of space navigation will take quite a long time, and the interval will contain an untold number of technological revolutions. But I believe that by the time of a communist society, we will certainly be able to master space navigation technology.

The future of our space navigation society is a bright one! Congratulations on the founding of JOURNAL OF THE CHINESE SOCIETY OF ASTRONAUTICS!

9432
CSO: 8111/0662 A

STRESS ANALYSIS OF BOTTOM STRUCTURE OF CYLINDRICAL SILO

Nanjing NANJING GONGXUEYUAN XUEBAO in Chinese Dec 79 pp 1-9

[Article by Song Qigen [1345 0796 2704] for the Teaching and Research Section of St.uctural Mechanics, NIT; and Yuanzhou Coal Mine Design Office: "Experimental Study and Theoretical Analysis of the Bottom Structure of a Cylindrical Silo"]

[Text] Abstract

This paper covers the stress analysis of the bottom structure of a cylindrical silo with a 3,600-ton capacity. This bottom structure is composed of two diagonal V-type folded plates and four conical shell panels (Figure 2). The 1:25 scale model test on a model of polymethyl methacrylate is described. Analysis based on the finite element technique and an approximate method which can be used in preliminary design are also presented. The results of calculation are compared with the experi ent data.

I. Summary of Experimental Study of Model

The experimental study of model is designed for the extension of a cylindrical coal silo at Lujiantuo, the Kailuan Coal Mines. The bottom structure of the silo consists of two diagonally placed V-type folded plates which are mutually perpendicular and four conical and shell panels fitted in the fan-shape spaces between the folded plates and silo wall (Figures 1 and 2). The silo has a capacity of 3,600 tons, is 37.75 meters high and 15 meters in diameter. The whole structure sits on a M-type conical shell foundation supported by 12 posts. The geometric scale of the model is 1:25 of the actual life size of the silo (using only a portion of the silo wall). Its shell is 1 cm thick, not quite adequate for simulation purposes. The model is built of polymethyl methacrylate ($E = 2.93 \times 10^4$ kg/cm^2, μ=0.39). It has greater strain values and is easily molded in processing. The seams of the model are glued tight with chloroform. The model has been put through the following two load tests:

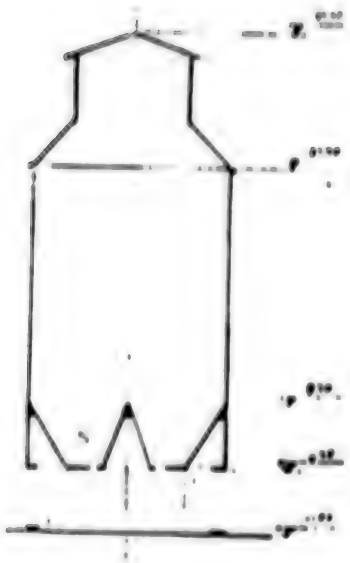

Figure 1.

1. Load of atmospheric pressure. The experimental findings are compared with theoretical analysis. The atmospheric pressure is applied manually in three stages. To allow greater strain value to distribute to a maximum number of resistor plates, the maximum load used is 0.6 atmospheric pressure (generally not exceeding 1000 microstrain so as to avoid gradual strain). A 5mm thick rubber gasket is placed between the steel lid of the model and the model itself to insure tight sealing and they are clamped together with 28 bolts (Figure 2). The resistor plates inside the model are connected to the lead-out wires built inside the silo wall. Approximately three working resistor plates share one compensating resistor plate which skips to radiate heat.

2. Experimental study of pressure load of porous material. To stimulate coal pressure, the load applied through levers is distributed to the model through a 25mm thick sand cushion. The load increases in 3 stages and maximum load is 3000kg. A plastic film sack is placed between the sand and the model to prevent damage to the resistor plates by direct contact with the sand. Everything else is the same as in the loading of atmospheric pressure.

The distribution of test points. Since the symmetrical surfaces in the structure run in longitudinal and latitudinal directions at a 45° line, the test points are distributed within one-eighth of the whole area as Figure 3. (The test points distributed on the silo wall, the circular rim and the posts are not shown in this figure.) Test results are marked "X" in the following related figures.

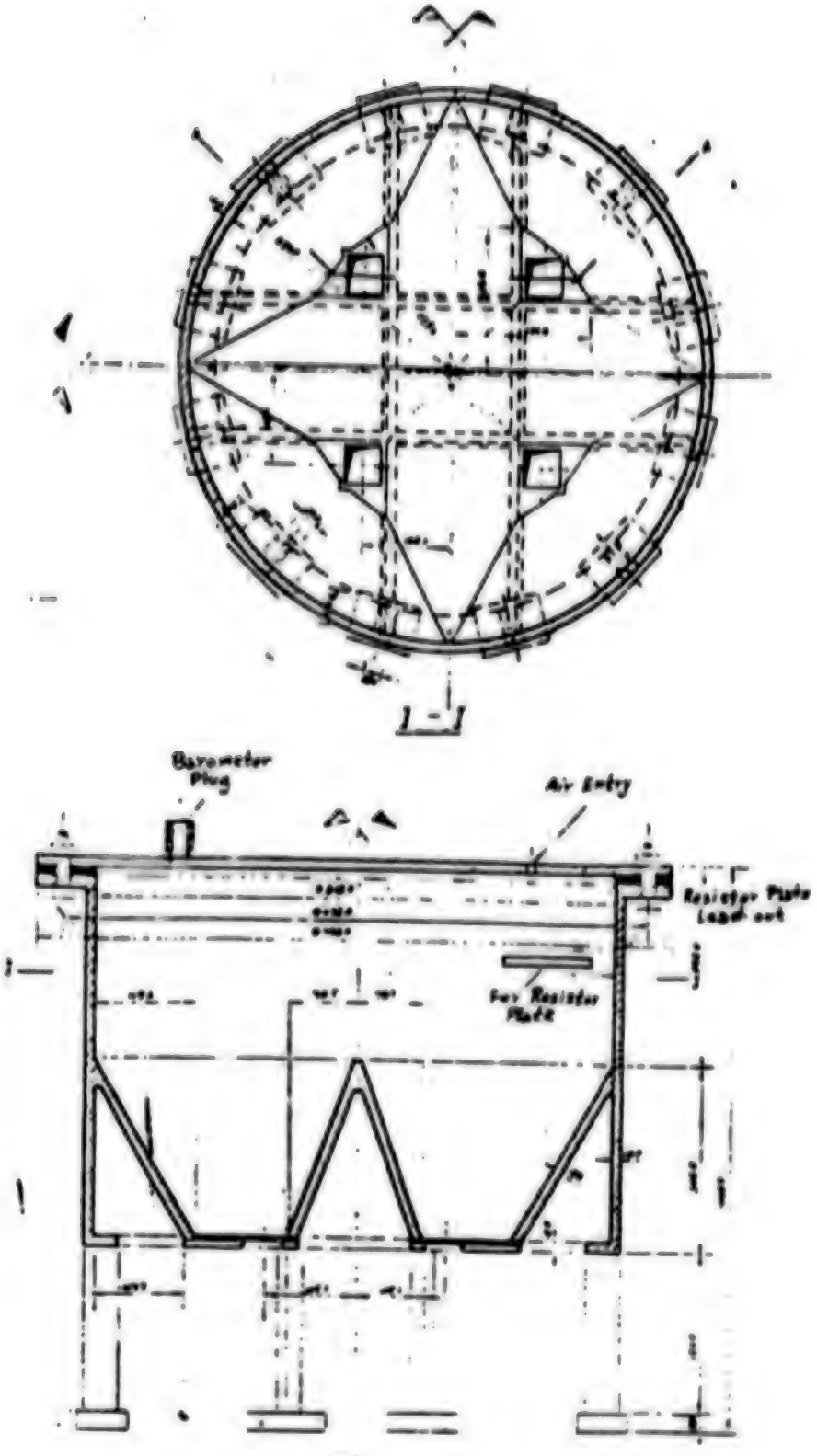
Barometer Plug
Air Entry
Resistor Plate Lead out
Fan Resistor Plate
A-A

Figure 2.

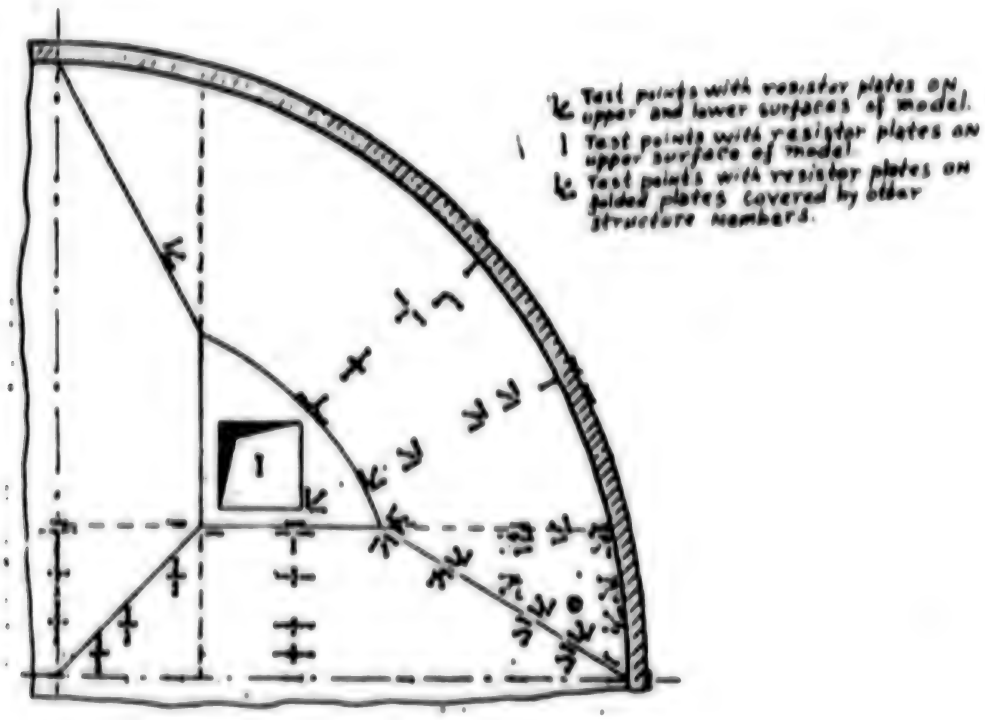

Figure 3. Distribution of test points on model

II. Computation by the Finite Element Method

The computation should be in keeping with the working of the entire structure. Any effort to meet the border and connection requirements should be as compatible as possible with the actual condition of the structure. The computation may proceed by "The Finite Element Technique for Combined Plate Shell and Lever Structures."[6] The conical shells, folded plates and silo wall are considered as thin shell members. The circular rim and posts are regarded as nonelastic space levers. Due to limited capacity of the computer, only that portion of the silo wall above the folded plates adjacent to the funnel is included in the computation.

Planar triangular units are used for shell structure members. The displacement module due to planar stress is the linear equation of the two component vectors of the middle plane. The displacement module due to curved stress is the cubic equation of yielding (normal displacement). Each nodal point in a unit has six degrees of freedom. When comparing the above simple units with more complex units which command even more degrees of freedom, it would be better to use a more dense unit-web. The unit size may be smaller than the radius of the curve, thus making the curves formed by the planar units not too much smaller than the curves of the original structure. Since the power of the equation of this displacement module, especially the part under planar stress, is comparatively low, calculation accuracy is poor.

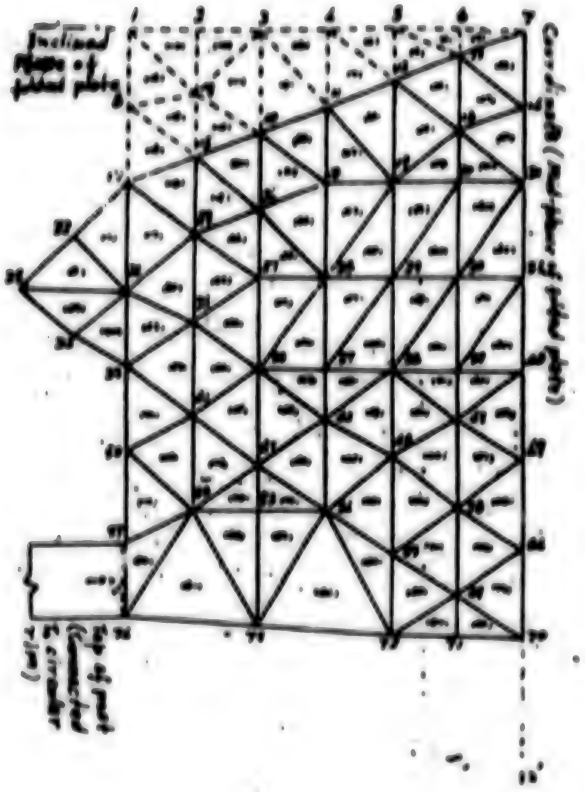

Figure 4.

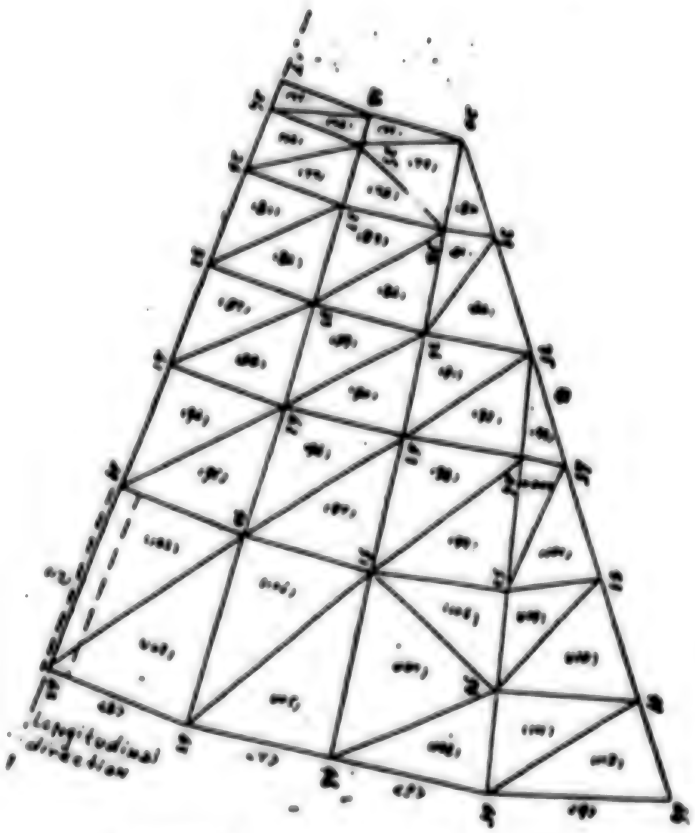

Figure 5.

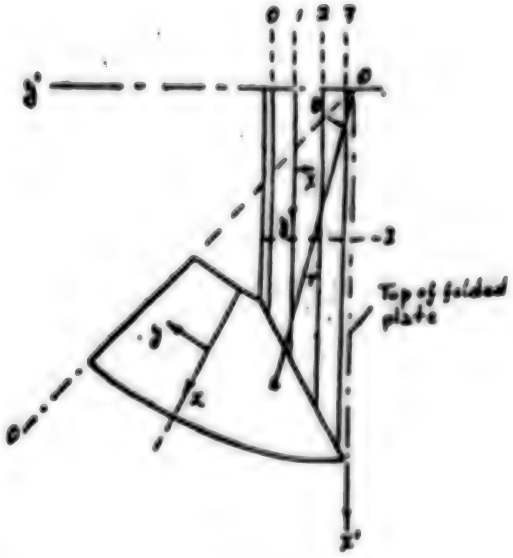

Figure 6.

1. Cases of calculation and unit-webs

Case 1. The unit is evenly divided (Figure 4 shows portions of the folded plates) into 166 surface units. The parts of the folded plates directly under pressure is the most important point for calculation. For the displacement of the nodal points in the cross section of the posts (such as point 57 and point 74 of Figure 4) to agree with the deformation of planar section of the posts, hypothetical rigid rods (such as Rod 12 in Figure 4) are placed between these nodal points. The calculated results are indicated by solid lines in Figures 7 and 8 (the locations of the section and parts of the coordinates are in Figure 6).

Case 2. There is a total of 156 planar units. The conical shell and the covered portion of the folded plates are the important points for calculation (unit divisions of conical shell are shown in Figure 5). In addition to the hypothetical rigid rods to insure displacement coordination, the following structural details are also considered (Figure 2):

(1) The top tip of the folded plate is regarded as the trapezoid section of a rod.

(2) The reinforced part of the joint formed by the widened lower border of the folded plate, the conical shell and the silo wall is considered a rod.

The results of the calculation in this case are shown by solid lines in Figures 9, 10, 14, 18 and 19 (the locations of the cross sections are shown in Figure 6).

The choice of the rigidity of the hypothetical rods calls for further studies. Theoretically, the rigidity chosen should be infinity. However, extremely high rigidity leads to calculation errors. The choice of this article is close to 10,000 times the rigidity of the structural parts.

2. Sorting and analysis of calculation results.

The internal forces obtained by the computer include the planar stress on the triangular surface, the curved stress on the four points (the center of the symmetry and the three points of the triangle), and the internal force at both ends of the rod. The true internal force of the structure may be derived from a study of these findings. Due to lack of precision in the divisions of the unit, the low power of the displacement equation and the substitution of folded surface for curved surface, the stress on the adjoining units vary considerably (especially where stress variation is great). The stress at a particular point calculated from different units varies noticeably (i.e. a lack of stress continuity between the units). Therefore, the internal force exerted at the symmetric center of two adjacent units represents the true internal force of the structure at that particular point.

The actual internal force of the rod which connects the planar unit along the length of the rod is the internal force of the mid section of the rod calculated from the internal force at its end. The true internal force of the rod which connects the planar unit at its end is the internal force at the rod-end calculated by computer.

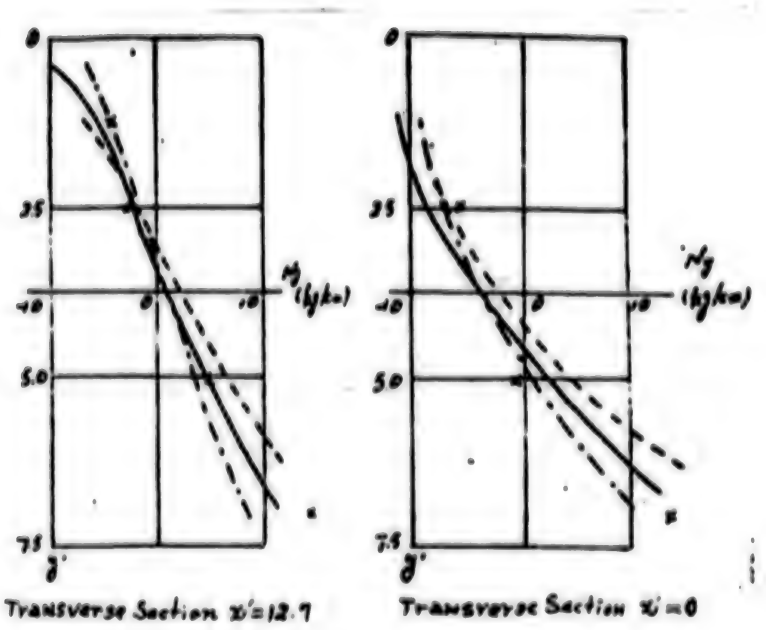

Figure 7.

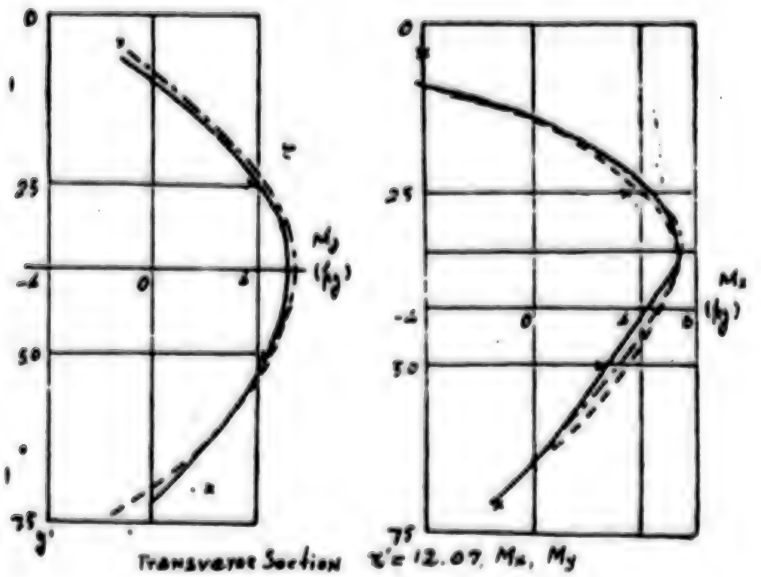

Figure 8.

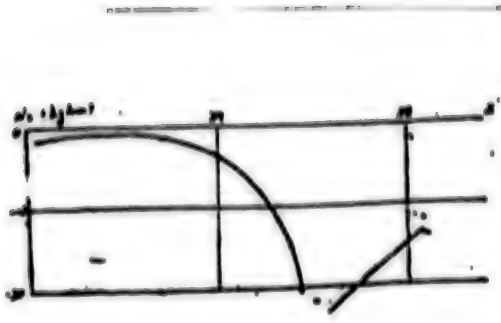

Vertical Section, folded plate O

Figure 9.

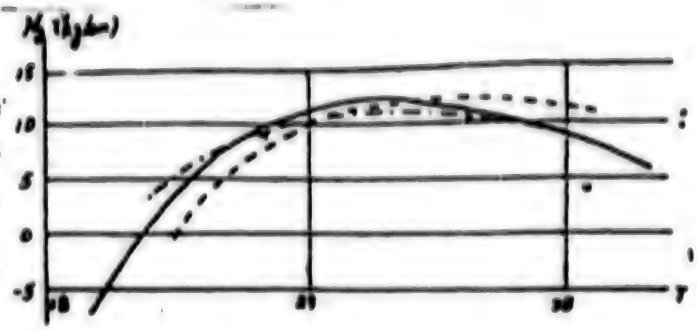

Longitudinal Section, Conic Shell $\theta = 0°$

Figure 10.

The typical representations shown in Figures 7-10 and Figures 14, 18 and 19 demonstrate that the overall calculated results agree with the experimental data. But the experimental value of the vertical torque of the folded plate next to the circular rim (near units 75 and 80 in Figure 4) is much higher than the calculated value. The cause for this marked discrepancy calls for further studies.

III. Calculation by Approximate Analysis

The whole structure is approximately divided into two groups for purposes of calculation. (1) The folded plates, the circular rim, the posts and the silo wall are regarded as one unit of calculation (the silo wall is not shown in Figure 11). The external forces of the circular rim and the posts are determined by approximating the interaction between all the structure members. (2) The conical shells, the silo wall and the small horizontal base board (BGC in Figure 12) are considered another unit.

The impact of the folded plates must be approximated while calculating the conical shells. These two calculation units are explained as follows:

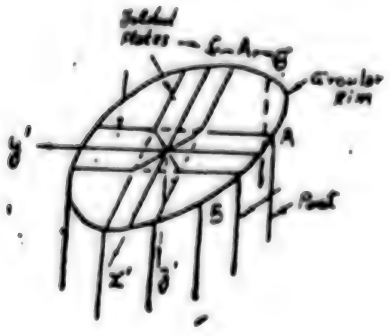

Figure 11.

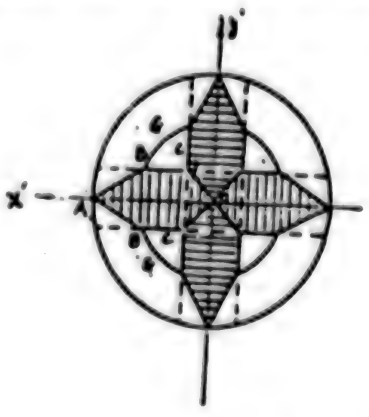

Figure 12.

1. The calculation of the folded plates, the circular rim and the posts. The folded plates are calculated by the approximation method which is known to the designers and does not require any further explanation. The internal forces of the circular rim and posts can be calculated by the displacement method of the system shown in Figure 11. Since the planar rigidity of the folded plates is very small the supporting structure and the coordination of displacements along the vertical axles of the folded plates are the only points to consider. When the cross section of the folded beam rotates $\theta_y = \omega$(Figure 13), nodal point A (Figures 11, 13) also rotates ω and produces vertical direction displacement (H is the height of the folded plate). Where the resistance of the folded plates, the circular rim, the posts and the silo wall to these displacements and the torque of the fixed ends of the folded plates are known (assuming that the folded plates are subject to the load shown in shaded area of Figure 12), then the displacement of nodal point A can be determined and finally the internal forces of all the structural members are ascertained.

The circular rim is planar round rod while the folded plate may be regarded as a beam. So the resistance of the circular rim, the folded plates and the posts is not too difficult to determine. The elastic resistance of the silo wall may be determined by approximation according to the theory given in.[2] Assuming that the interacting force between the folded plates and the silo wall is p distributed along a straight line of its height, i.e. $p = \alpha + \beta_z$, the displacement at point A on the silo wall caused by p in x' direction along generatricies E, E', F, F' can be obtained from the following equations based on integrated increments of the solutions given in[2]:

$$\Delta = \sum_{n=1,2\cdots} 2f_n(\cos\theta_1 \cos n\theta_1 + \sin\theta_1 \sin n\theta_1/n) \qquad (1)$$

$$f_n = \frac{a^3}{\pi D l (n^4-1)} \cdot r\left\{2\alpha H + \frac{1}{2}(\beta + \alpha\varrho_n z)\left[l^2 - (l-2H)^2\right] + \frac{\beta\varrho_n z}{3}\left[l^2 - (l-2H)^2\right]\right\} \qquad (2)$$

Where a in the equation is the radius of the mid section of the silo wall and D is the rigidity against bending, then $\varrho_n = \frac{n^2}{n^2\ell^2/3 + 2(1-\mu)}$, μ=Poisson's ratio.

Assuming that the axle of the folded plates does not extend and rotating angle of the silo wall is ω, then: $\Delta|_{z=\ell-H} = 0$, $d\Delta/d_z = \omega$,

Both α and β can be obtained from these and the resistance of the silo wall can be calculated from p.

After obtaining the rotating angle ω of the top cross section of the folded plates, the internal force of the circular rim and the posts as shown by dotted lines in Figure 14 (solid lines represent results of the finite element method) and Table 1 can be obtained.

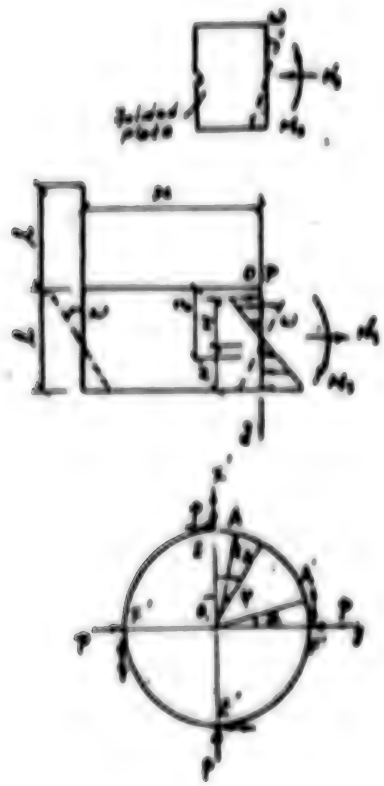

Figure 13.

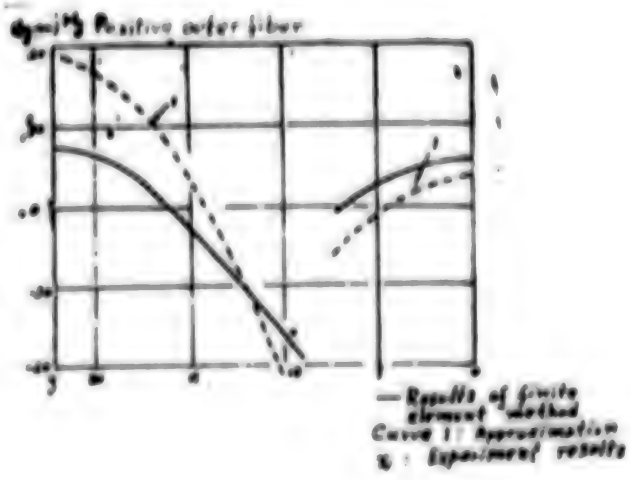

Figure 14.

Table 1. Comparison of Internal Force of Post A

	Post Top Cross-Section				Post Bottom Cross Section	
	P_y	P_z	M_y	M_z	M_y	M_z
Results of Approximation Method	7.50	-2.01	21.0	78.3	15.2	56.7
Results of Finite Element Method	8.18	-1.84	22.9	81.4	11.1	70.0

(Cylindrical cross section of main axle Z along the direction of the intersection line of the silo wall)

2. Conical shell calculation

The horizontal lines at the upper and lower borders of the conical shell panel contact the silo wall and the small horizontal board in the funnel area. This provides elastic support. The contact line between its side border and the folded plate is not a vertical line. This kind of conical shell panel is difficult to analyze minutely. To calculate properly, the border factors have to be greatly simplified in order to do an analysis according to the mid-length shell approximation theory.[1] Treat the total stress on the conical shell as the combination of homogeneous integration and the increment of the internal force of the membrane. The theory of homogeneous integration[1] might be proven by expanding the orthogonal function series. Thus, the elastic support at the loop border can be simplified as follows: The lower border CD is regarded as simple support, i.e., when $\alpha = \alpha_1$, $T_1 = \upsilon = 0$ (Figure 15). The border factor at the upper edge AB ($\alpha = \alpha_2$) is assumed to be related to the load, i.e. when the load is horizontal, $T_1 = \upsilon = 0$ and when the load is vertical $u = \upsilon = 0$. These factors determine both the characteristic function $\Phi(\xi)$ and the characteristic value x.

The hypotenuse in contact with the folded plate may be replaced by a suitable longitudinal line. The circular intersecting line of the conical shell panel can also be approximately considered as the normal line of the folded plate. Of all the four border factors, the one involving circular force T_2 is the most important. Therefore the border factors can be equated as:

$$\text{When} \quad \theta = \theta_2, \quad T_2^* + T_b + Q_b^0 = 0, \qquad u^* = w^* = \gamma_z^* = 0 \tag{3}$$

then $T_2^* = T_2 + T_2^0$, $u^* = u + u_0$, etc. T_2 etc. are obtained by homogeneous integration, and T_2^0 etc. by membrane integration which may be calculated according to prepared schedule. The elastic resistance of the folded plate, T_b, is caused by the displacement υ^* on line BD. The counter force of the folded plate, Q_b^0, is produced by the surface load when BD is the immobile support (Figure 16). Because it is difficult to calculate the force of the trapezoid plate when the three sides are supported and one side is hung in suspension, Q_b^2 is obtained by approximating the counter force on the hypotenuse of the three-sides of the congruent triangle (using prepared schedules). To make the calculation more manageable, assume by approximation that T_b is distributed along BD (Figure 17) and that under the evenly distributed load, q = 1, along BD the yielding of the folded plate at BD is δ, then

$$T_b \cdot \delta = \upsilon^* \tag{4}$$

In calculating δ, the DD^1 side of the folded plate is considered fixed, DF and D^1F^1 are considered simple side support and FF^1 is considered in suspension (though supported at BB^1). Since the variability of δ thus obtained differs from υ^*, equation (4) is not very helpful. So the T_b is determined by a minimum error square.

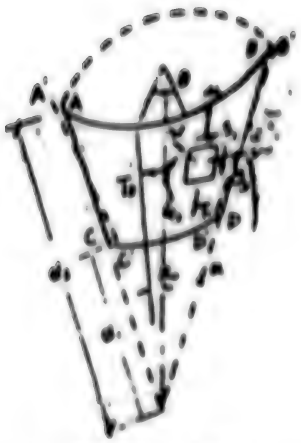

Figure 15.

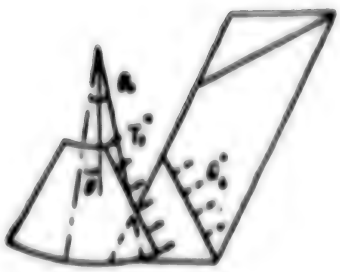

Figure 16.

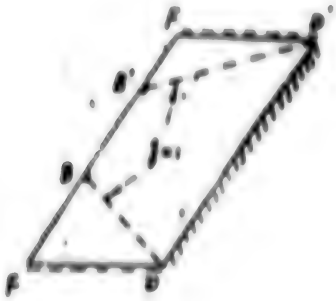

Figure 17.

The mid-length shell theory[1] overlooked G_1, the vertical torque of the conical shell. Since the conical shells covered in this article are comparatively short, a modified calculation procedure is required for G_1. An approximation of G_1 from G_2 is as follows:

$$G_1 = \frac{\mu\lambda^2 + (\chi \sin \chi_0)^2 \sqrt{\rho}}{\lambda^2 + \mu(\chi \sin \chi)^2 \sqrt{\rho}} G^2 \qquad (5)$$

As shown in the equation, χ_0 = half open interval of the conical shell panel (Figure 15), $\rho = i g_{\chi 0}/\sin^4 \chi_0$, $\lambda^4 = \chi^2\, 3(1-\mu^2)R_0^2/h^2$ See reference (1). The total stress on the conical shell as shown by dotted lines in Figures 18 and 19 can be obtained from the above calculation plus the increment of the simple margin effect at the circular border. Due to the fact that conical shell edge on the symmetrical plane (θ = 0) is supported by posts (Figure 2), calculation by approximation is hard to apply here. Although this zone is far away from the hypotenuse of the conical shell, the results obtained by the approximate method differ rather noticeably from those obtained by the finite element method.

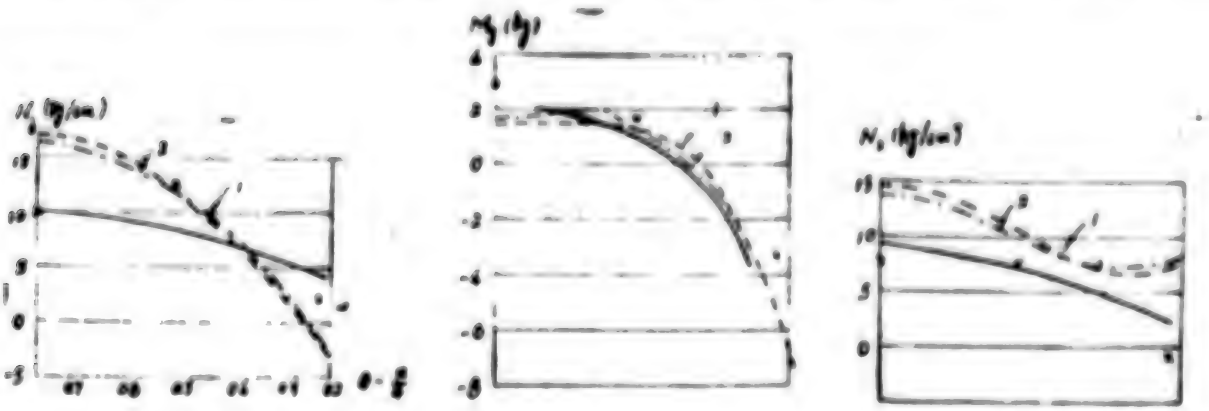

Figure 18. Circular section = 22.15

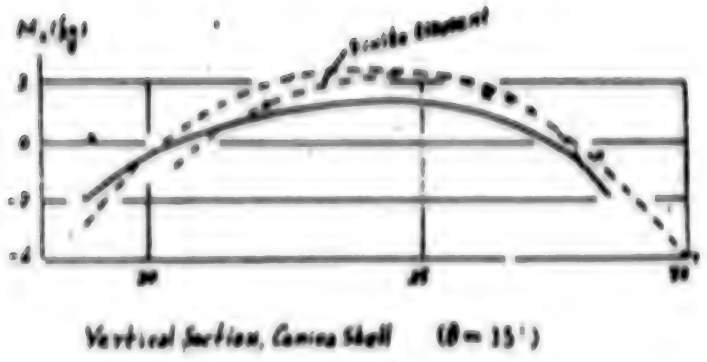

Vertical Section, Conical Shell ($\theta = 15°$)

Figure 19.

REFERENCES

1. A. L. Gol'denveyzer: The Theory of Elastic Thin Shell, Ch 18, Sect 21, 22; Ch. 17, Sect 12.

2. S. Timoshenko et al: The Theory of Plate Shell, Sect 120, 1977.

3. Zienkiewicz et al: The Finite Linear Equation in Structural and Continuous Mechanics, Translation by Jiaotong University, Shanghai, 1973.

4. East China Institute of Water Conservancy: The Finite Element Methods in Elastic Mechanics, 1974.

5. I. Holand et al: Finite Element Methods in Stress Analysis, 1972.

6. Yuanzhe Coal Mine Research Design Institute, Ministry of Coal Industry and Fifth Department, Nanjing Institute of Technology: The Finite Element Technique in Combined Plate Shell and Lever Structures, NANJING GONGXUEYUAN XUEBAO, 1978, 2.

5360
CSO: 8111/0599A

PUBLICATIONS

TABLE OF CONTENTS OF 'GUTI LIXUE XUEBAO' NO 2, 1980

Hubei GUTI LIXUE XUEBAO [ACTA MECHANICA SOLIDA SINICA] in Chinese No 2, 1980 p 286

9717
CSO: 4008

TABLE OF CONTENTS OF 'FUDAN XUEBAO (ZIRAN KEXUE BAN)' NO 3, 1980

Shanghai FUDAN XUEBAO (ZIRAN KEXUE BAN) [FUDAN UNIVERSITY JOURNAL (NATURAL SCIENCES)] in Chinese Vol 19 No 3, 1980 p 238

9717
CSO: 4008

PUBLICATIONS

TABLE OF CONTENTS OF 'GANGTIE' NO 9, 1980

Beijing GANGTIE [IRON AND STEEL] in Chinese No 9, Dec 80 preceding p 1

9717
CSO: 4008

PUBLICATIONS

TABLE OF CONTENTS OF 'DIANZI JISHU', DECEMBER 1980

Shanghai DIANZI JISHU [ELECTRONIC TECHNOLOGY] in Chinese No 12, Dec 80 p 48

[Text] Table of Contents

9698
CSO: 4008

AUTHOR: ZHENG Yingren [6774 4481 0086]

ORG: None

TITLE: "Approximate Calculation of Stress and Boundary Line of the Plastic Region of Rocks Surrounding a Round Cave"

SOURCE: Chongqing DIXIA GONGCHENG [UNDERGOUND ENGINEERING] in Chinese No 3, 11 Mar 80 pp 1-7

ABSTRACT: At present, under the condition of equal initial stress in all directions in the strata (i.e. $\lambda_0 = 1$, λ_0 being the side pressure coefficient) the stress field and its boundary line of the plastic region of rocks surrounding a round cave can be obtained completely with analysis method. If the vertical initial stress and the horizontal initial stress are not equal ($\lambda \neq 1$) then the stress field and the boundary line can be obtained numerically with the aid of the finite unit method only and different methods of concrete computation may produce different results. This paper proposes 2 methods of approximate calculation. Following detailed analysis, it is also suggested that in actual application, the result of the second method here proposed should be adopted.

AUTHOR: YANG Muhuai [2799 1970 2037]

ORG: None

TITLE: "Several Problems Concerning Excavation and Support of Dirt Caves"

SOURCE: Chongqing DIXIA GONGCHENG [UNDERGROUND ENGINEERING] in Chinese No 3, 11 Mar 80 pp 7-10

ABSTRACT: With a large quantity of underground engineering projects for railways, water conservancy, hydroelectrical power, mining, or defense, the work does not necessary proceed through various dirt, rock, or salt media. Sometimes, the work is entirely done under soils. The problem of interaction between the underground structure and the medium of its site remains the same, however. The problem involves the method of handling the pressure exerted by the medium onto the structure and the capacity of the medium to bear the load of the structure. This is an extremely complex problem awaiting urgently for a solution. This paper discusses that portion of the problem concerning the excavation of caves in soil strata and the method of providing adequate supportive measures. Several viewpoints are offered.

AUTHOR: LI Huemu [2621 0129 4476]

ORG: None

TITLE: "Preliminary Application of Hydraulic Lift Scaffold in Underground Engineering Projects"

SOURCE: Chongqing DIXIA GONGCHENG [UNDERGOUND ENGINEERING] in Chinese No 3, 11 Mar 80 pp 10-11

ABSTRACT: The new technique of using hydraulic lift scaffold has been preliminarily adopted in the projects of constructing underground oil tanks in the last 2-3 years. Instead of placing the steel framework inside of the concrete oil tank, the molded scaffolding platform is fastened outside of the tank and moved up and down by a hydraulic lift. This paper explains the technique and the structure of this new work tool. A preliminary estimate indicates a saving of 3250 man/day of work and about 13,000 yuan in cost for every oil tank constructed with this tool.

AUTHOR: BIN-TIAN Zhengze [3453 3944 2398 0463] [Transliteration of a Japanese Name]

ORG: None

TITLE: "Dynamic Observation and Analysis of a Large Underground Oil Tank During an Earthquake"

SOURCE: Chongqing DIXIA GONGCHENG [UNDERGOUND ENGINEERING] in Chinese No 3, 11 Mar 80 pp 40-54

ABSTRACT: In recent years, large undergound tanks are being constructed everywhere to store liquid gas, crude oil, etc. There has not been a sufficiently long historical background for these structures to undergo the test of large earthquakes and especially, most of these are built in soft and weak foundations of the coastal regions. This paper reports a seismic observation by the author of underground oil tanks actually in use to study the dynamic relationship between the strain of the side wall of the tank and the surrounding foundation during an earthquake. This paper originally appeared in A COLLECTION OF CIVIL ENGINEERING PAPERS [in Japanese?] No 273, 78 pp 1-14 and translated into Chinese by CHEN Cailai [7115 2088 0171] for this journal.

6248
CSO: 4009

AUTHOR: ZHU Jinnin [2612 2417 3046]
BAI Yuanchang [4101 0337 1603]

ORG: None

TITLE: "Comprehensive Discussion of Rock Cave Stability Analysis and Designing and Construction of the Support Structure"

SOURCE: Chongqing DIXIA GONGCHENG [UNDERGOUND ENGINEERING] in Chinese No 12, 11 Dec 80 pp 1-20

ABSTRACT: In the past 3 decades, application of undergound engineering structures has grown rapidly in kinds as well as scale, in China as well as in foreign countries. Whether or not the capital investment of such projects can be reduced, the construction duration can be shortened, and the construction and use of such structures can be made safe depend, to a very large extent, upon a rock stability analysis, which is a complex problem. It is closely related to engineering geology, petro-mechanics, and design engineering. This paper attempts to use domestic and foreign large span rock cave projects as examples to discuss the mechanical characteristics of rocks and rock bodies, the method of analyzing the stability of the adjoining rocks, the method of designing and computing the support structure, the application of classification of tunnel adjoining rocks, and the method of strengthening adjoining rocks.

AUTHOR: LUO Wenbao [5102 2429 6283]

ORG: None

TITLE: "Reasonable Method of Designing Supports for Loessical Caves"

SOURCE: Chongqing DIXIA GONGCHENG [UNDERGOUND ENGINEERING] in Chinese No 12, 11 Dec 80 pp 21-28

ABSTRACT: The loessical strata are mainly sedimentary strata by wind power in the Quaternary Period. Its characteristics include large crevices, with vertical cleavages and pipe-like pores, but capable of maintaining very high vertical slopes. The soil is mainly composed of powder-like grains of 0.05-0.005mm in diameter, with a rich carbonate content and calcium nodules. In Northwestern China, the total loess distribution is 440,000 km^2 and the deposit is more than 200m in thickness in some places. In recent years, many tunnels and caves have been constructed in this loessical region. The practice demonstrated that the key to success is the stability of the support structure, which occupies the major portion of the cost of an entire cave. Following an extensive discussion of several currently available or classic methods of designing, an experimental formula, summarized from the experience of 93 engineering projects of this type, is offered. When the support structure is designed in accordance with the formula, safety and relative economy may be guaranteed.

AUTHOR: MOSTKOV, V. M.
REZNIKOV, R.A.

ORG: None

TITLE: "The Static Force Computation Method of the Main Underground Machine Chamber of a Hydroelectric Station"

SOURCE: Chongqing DIXIA GONGCHENG [UNDERGROUND ENGINEERING] in Chinese No 12, 11 Dec 80 pp 63-67

ABSTRACT: This paper discusses at length the theory of comprehensive method of analyzing the stress-strain phenomena of adjoining rocks of a large underground tunnel and the guarantee of its stability. The method is summarized in 10 stages. This paper originally appeared in GIDROTEKHNICH STR-VO [HYDROTECHNIQUE] [in Russian ?] No 1, 79 pp 20-23. It is translated into Chinese for this journal by XU Xianyi [1776 7359 3015].

6248
CSO: 4009

AUTHOR: HUANG-FU Dexing [4106 3940 1795 5281]

ORG: None

TITLE: "Pumping Water to Store Energy Power Stations Under Development"

SOURCE: Beijing KEXUE SHIYAN [SCIENTIFIC EXPERIMENT] in Chinese No 1, 81 pp 16-17

ABSTRACT: Pumping water to store energy is a well developed concept in such industrially advanced countries as the USA, Japan, and in Europe. In China, it has just begun. The surplus power during a flood season or at midnight is used to pump water to a high reservoir or a regulating tank so as to exchange the head for electrical energy on demand. This type of power station is in reality a versatile power storage tank. This paper explains the many forms of using surplus power to pump water for the purpose of storing energy. In China, the highest head thus created is 65 m in Miyun Reservoir, with a single machine capacity of 12,800 kw. Further development of this technology is being planned.

AUTHOR: MA Huilin [7456 1920 2651]
WU Peinin [0702 1014 1380]

ORG: None

TITLE: "Power Generation Atop of a Blast Furnace"

SOURCE: Beijing KEXUE SHIYAN [SCIENTIFIC EXPERIMENT] in Chinese No 1, 81 pp18-19

ABSTRACT: In a thermal power plant, water is changed into steam to produce electric power. When iron is being refined in a blast furnace, hot air is blown from the lower part of the furnace to cause the carbon in the coke to react with the oxygen in the hot air to produce a gas. The interaction between the burning gas and the ore will result in the continuous rise of the gas and settling of the ore. Iron is thus separated from the slag. When a large quantity of hot air is blown into the furnace and when a certain energy level is reached, a pressure-reduction valve atop the furnace will automatically open to release the surplus energy to keep the pressure in the furnace at a safe level. In 1974, a Japanese steel mill was the first to utilize this surplus energy to generate power. By Sep 79, 21 blast furnaces in Japan had adopted this technique. It is estimated that the power used by one million two hundred thousand households have thus been generated.

6248
CSO: 4009

AUTHOR: HAO Pengyin [6787 7364 0603]

ORG: Deputy Chief, Division of Production, Ministry of Coal

TITLE: "Total Quality Control (TQC) Should be Developed More Vigorously in the Coal Mining Industry"

SOURCE: Beijing ZHILIANG GUANLI [QUALITY CONTROL] in Chinese No 6, 29 Dec 80 p 1

ABSTRACT: The energy utilization rate of coal is above 65 percent in Japan and only 28 percent in China. The high waste rock content of the coal causes a waste transport capacity of 40 million tons per year. About 50 percent, i.e. one hundred million tons, of coking coal is used as power coal in China. To overcome these unreasonable conditions, the author proposes (1) Establishing the principle of production; (2) A quality responsibility system; (3) Using modern scientific management methods; (4) Establishing methods of scientific planning and work; (5) Fully generate mass support. He also calls for a mobilization of all plants and workers to guarantee the users that the best possible products will be produced.

AUTHOR: None

ORG: Machine Work Section No 5, Paper-making Machine Shop No 2, Tianjin Paper Plant

TITLE: "How Did We Catch Up With Jincheng"

SOURCE: Beijing ZHILIANG GUANLI [QUALITY CONTROL] in Chinese No 6, 29 Dec 80 pp 14-15

ABSTRACT: The Machine Work Section No 5 makes the No 2 cardboard used in double-face printing. The annual production is 12,000 tons. There are 83 workers and the equipment is the 1930's style ordinary paper-making machine, which was made in 1958. The unrest of a decade had resulted in confusion of management and serious deterioration of quality. In 1977, the TQC experience of Japan was adopted to apply mathematical and statistical methods to production. After some strenuous efforts, the various quality indices have now reached the best level in the plant's history. It has now caught up with the quality level of Jincheng Paper Mill No 5 and No 6 of Liaoning, which are the most advanced in the nation. The concrete measures adopted are described.

AUTHOR: LUO Peihuan [5012 1173 3883]

ORG: Qianjiang Sugar Plant, Guangxi Province

TITLE: "Do a Good Job of Civilized Production to Improve the Quality of Sugar"

SOURCE: Beijing ZHILIANG GUANLI [QUALITY CONTROL] in Chinese No 6, 29 Dec 80 p21

ABSTRACT: Everyone knows about the saying "disease enters the body through the mouth." The quality of foods directly affects the health of the people. Qianjiang Sugar Plant is new, with new equipment and new workers. It is, therefore, essential to teach civilized production method. For example, pieces of cotton that had been used to clean the machine or pieces of rags that had been used to mop the floor should be absolutely kept from being mixed into the sugar to affect its quality. At one time, insoluble foreign substance was found to fluctuate between 100-200mg/kg, exceeding the standard set by the ministry. Through dissolution and magnetic absorption tests, the foreign substance was proved to be pieces of rusted iron. Further analysis and inspection disclosed the fact that the pipes connecting the evaporation tanks were not cleaned thoroughly to cause the rust to flow out with the syrup. A thorough cleaning of all the tanks and pipes brought about a great improvement of the quality of the sugar. These and other experiences of the plant are told.

6248
CSO: 4009

AUTHOR: ZHOU Jiu [0719 3773]
HUANG Xiuwu [7806 0208 2976]

ORG: Both of Sichuan Seismological Bureau

TITLE: "The Gravitational Plastic Flow of Crustal Materials in Southwest China"

SOURCE: Beijing DIZHEN DIZHI [SEISMOLOGY AND GEOLOGY] in Chinese No 4, Dec 80 pp 1-10

TEXT OF ENGLISH ABSTRACT: Under the action of gravity, the powerful driving forces of recent tectonic movement affecting the studied plateau and adjacent areas are stemming from the crust of the Qinghai-Xizang Plateau. Therefore, a flow of crustal materials toward the southeast took place in southwest China. Such a flow possesses a rather special nature, unlike the downhill sliding of the glacier. In the front of the flow can be found recent tectonic activities with different features due to the variations of resistance encountered. In addition, the occurrence of earthquakes in southwest China is also constrained by the material flow.

The authors suggest that, since the driving forces of recent tectonic activities in this area are closely related to the gravitational effect, the localized recent tectonic processes would be ascribed to the category of gravity tectonics.

AUTHOR: ZHANG Shiliang [1728 0013 5328]
CHEN Shangfu [7115 0006 4395]

ORG: Both of the Institute of Geology, National Bureau of Seismology

TITLE: "Analysis of Active Faults in Taiwan Province and Their Relation to Earthquakes from Satellite Images"

SOURCE: Beijing DIZHEN DIZHI [SEISMOLOGY AND GEOLOGY] in Chinese No 4, Dec 80 pp 11-20

TEXT OF ENGLISH ABSTRACT: Based upon the Landsat images, this paper briefly describes the active faults in Taiwan and their relation to earthquakes. The active faults, elongated mostly in a form of belt with distinct tectonic activity, are clearly characterized by the satellite images. The region under investigation is principally controlled by the NNE trending activa fault zones, which usually have a left-lateral character. Although the NW trending active zones are not as large on the scale as are the former, they behave as a fault with evidence of recent movement in northern Taiwan and are right-lateral in nature. By synthetic analysis of data concerned, this region is determined to be compressed from the NNW-SSE direction due to the collision between the Phillippine Sea plate and the Eurasian plate.

AUTHOR: AN Ou [1344 2962]

ORG: Seismogeological Expedition, National Bureau of Seismology

TITLE: "About the Deformation, Creep and Hysteresis in Rocks at Various Temperatures"

SOURCE: Beijing DIZHEN DIZHI [SEISMOLOGY AND GEOLOGY] in Chinese No 4, Dec 80 pp 21-26

TEXT OF ENGLISH ABSTRACT: The experimental results on rocks at a temperature equal to the earth's crust indicate that as long as a cyclic load is applied on rocks, there is no monodromic correlation appearing between stress and strain. Thus the recent tectonic stress and strain fields are changing, now extensively, now weakly. For this reason, it is impossible for the earth stress stations to maintain long-term continuous observation at the fixed points to evaluate the earth stress by the strain, and therefore a selective method for measuring the elasticity and a stress balance method are necessary in determining the stress state.

AUTHOR: YE Hong [5509 3163]
et al.

ORG: All of the Institute of Geology, National Bureau of Seismology

TITLE: "On the Source Tectonics of the 1979 Liyang Earthquake of Magnitude 6"

SOURCE: Beijing DIZHEN DIZHI [SEISMOLOGY AND GEOLOGY] in Chinese No 4, Dec 80 pp 27-38

TEXT OF ENGLISH ABSTRACT: In 1979 an earthquake of magnitude 6 occurred in Liyang County, Jiangsu Province. The epicenter was located in the junction of a NE trending active fault, the known Maoshan fault, with a NW trending active fault, the Fangshan-Tiger Mountain fault.

In this paper, the focal mechanism of the major shock and several aftershocks has been studied and the strike of seismic fracture has been determined by means of null vector data. The research results indicate that the Liyang earthquake was caused by a right lateral strike-slip dislocation with some normal dip-slip component along the east branch of the Maoshan fault belt under the action of the NEE compression stress field.

From the observation of aftershocks, it can be suggested that both the source volumes of the b-value of this earthquake sequence are rather small. Using the

[Continuation of DIZHEN DIZHI No 4, Dec 80 pp 27-38]

Wyss method and Gibowicz empirical formula, we estimated approximately the stress-drop and seismic moment as well as the apparent stress of the Liyang earthquake. In addition, based on the field geological observations, we pointed out tentatively that the Liyang earthquake was probably generated by the locked NE Maoshan fault associated with the left lateral shifting of the NE Fangshan-Tiger Mountain active fault. This seemed to be a reasonable explanation for the recurrence of two destructive earthquakes occurring there within five years.

The authors assume that the Liyang earthquake can be regarded as a low stress-drop event under a high stress background, implying that the southern part of the north China fault block has been stepping into an active stage of high stress.

AUTHOR: FANG Zhongjing [2455 0112 2529]
et al.

ORG: All of the Institute of Geology, National Bureau of Seismology

TITLE: "Geological Analysis of the Seismicity in the Tancheng-Lujiang Fault Zone, East China"

SOURCE: Beijing DIZHEN DIZHI [SEISMOLOGY AND GEOLOGY] in Chinese No 4, Dec 80 pp 39-45

TEXT OF ENGLISH ABSTRACT: This paper deals mainly with the geotectonic background of the seismicity in the Tancheng-Lujiang fault zone, with emphasis on the relationship of Late Quaternary active faults in the southern part of its middle segment to the earthquakes. The seismicity is clearly different in various segments. This is well correlated to the difference in geotectonic units with various characteristics and faulting activities in the Late Quaternary.

The evidence on the intermittent motion (stick-slip motion) of the active faults found in the southern part of the middle segment can be regarded as a geological indicator to discriminate the paleo-earthquakes and to roughly estimate their recurrence. It is clear that this indicator is of practical significance for evaluating the seismic tendency of the active fault zone. In addition, by the geological and seismological analogs the authors propose that, in the same

[Continuation of DIZHEN DIZHI No 4, Dec 80 pp 39-45]

tectonically active zone where strong historic or prehistoric earthquakes occurred, the possibility exists of recurrence of earthquakes in the same location. However, it is to be noted that some segments of this zone, where the tectonic conditions are similar in the occurrence of earthquakes and evidence of intermittent motion of active faults since Late Pleistocene are found and where seismic gaps last more than 2000 years, can be referred to as the temporal "quiet segments." The earthquake risks in these segments may actually be more serious than those in the segments with recent activity. Therefore, we should not say that the former segments will be safe in the near future. It has already been verified by the fact that in recent years quite a few strong earthquakes have taken place in the historical seismic gaps which were tectonically newly reactivated. In conclusion, in making the seismic zonation more exact one should pay attention to the investigation of the geologico-geomorphological evidence on recurrence of large earthquakes in the active fault zone within plates.

AUTHOR: HAN Mukang [7281 1970 1660]
ZHAO Jingzhen [6392 2529 3791]

ORG: HAN of the Department of Geography, Beijing University; ZHAO of Henan Seismological Bureau

TITLE: "Seismotectonic Characteristics of Tangyin Graben, Henan Province, and Its Earthquake Risk"

SOURCE: Beijing DIZHEN DIZHI [SEISMOLOGY AND GEOLOGY] in Chinese No 4, Dec 80 pp 47-58

TEXT OF ENGLISH ABSTRACT: The authors illustrate the characteristics of neotectonic movement of the Tangyin graben (Henan Province) situated in the southern section of the Taihanshan Piedmont fault zone with a NNE trend and point out that the northern part of this graben is only a semigraben, while its western side is a hinge fault with progressively decreasing vertical displacement, finally dying out in the northern direction. According to the field seismotectonic investigations, the authors made a prediction that the western part of Tangyin County near the hinge point is prone to earthquakes due to the hinge point's further northward migration. Later this prediction was verified by an earthquake of 3.9 M occurring in this part in October 1978.

In addition, Anyang City, located on the intersection of the Taihanshan fault

[Continuation of DIZHEN DIZHI No 4, Dec 80 pp 47-58]

zone with a NWW pivotal fault, is in another earthquake-prone area due to the feasible location to concentrate tectonic stress, and it should be monitored.

AUTHOR: LI Qinzu [2621 2953 4371]
JIN Yamin [7246 7161 2404]
YU Xinchang [0060 2450 2490]
et al.

ORG: All of the Hebei Seismological Bureau

TITLE: "Focal Mechanisms of Tangshan Earthquakes"

SOURCE: Beijing DIZHEN DIZHI [SEISMOLOGY AND GEOLOGY] in Chinese No 4, Dec 80 pp 59-67

TEXT OF ENGLISH ABSTRACT: In this paper some characteristics of the Tangshan earthquakes are discussed from the data of focal mechanisms. The fault plane of the main shock is a bilateral strike-slip fracture along N30°E and appears clearly to control the aftershocks so that the stronger aftershocks occurred concentratedly around the two stopping positions of the fault plane. This was determined by the distribution of remaining stress over the fault plane of the main shock after its occurrence. The larger differences of the fault plane solution of some aftershocks and the higher percentages of the inconsistent first motions in the composite fault plane solutions of aftershocks imply that the fractures and the redistribution of the stress in the focal region after the occurrence of the main shock were complicated. The decrease in the percentage of inconsistent first motions in the later composite fault plane solution shows a probable indication that the medium

[Continuation of DIZHEN DIZHI No 4, Dec 80 pp 59-67]

in the focal region was going from a strained equilibrium to a lax equilibrium. It was pointed out from the analysis of seismic data that the fault plane solution of the main shock is representative for most of the earthquakes in north China. Some information which is probably useful for the prediction of earthquakes is discussed.

AUTHOR: YIN Xiuhua [3009 4423 5478]
et al.

ORG: All of the Institute of Geology, National Bureau of Seismology

TITLE: "The Basic Features of the Regional Gravity Field in the Chinese Continent"

SOURCE: Beijing DIZHEN DIZHI [SEISMOLOGY AND GEOLOGY] in Chinese No 4, Dec 80 pp 69-75

TEXT OF ENGLISH ABSTRACT: The $1^{o}/1^{o}$ free-air anomaly and Bouguer anomaly of the Chinese continent can be briefly outlined by using 104^{o}E as a border line separating into the eastern and western parts which are distinctly different in anomaly features. The anomaly change of the former is gentle with a NNE strike of linear anomaly, while the latter's change is intensive with a NWW strike of linear anomaly. The further subdivision of the Chinese continent gives four anomaly regions: the Eastern, Central, Xinjiang and Qinghai-Xizang. They vary obviously in nature. We discuss the relationships between the regional gravity field and tectonics, isotasy and seismicity. It is suggested that the linear anomalies of the Eastern part mainly reflect the structural system of the NNE strike, but those of the Western part reflect the structural system of the NWW strike. The Bouguer anomaly gradient zones coincide with the fault belts between fault blocks, and

the Chinese continental crust is principally in an isostatic state on a large scale. Therefore it can be assumed that most of the earthquakes would take place along the gravity gradient zones.

9717
CSO: 4009

AUTHOR: Ni Zhaojing [0242 0340 0079]

ORG: None

TITLE: "A Technical and Economic Comparison of Television Satellite and Communications Satellite in the Domestic Satellite System"

SOURCE: Shanghai DIANXIN KUAIBAO [TELECOMMUNICATIONS INFORMATION] in Chinese No 9, 80 pp 1-8

ABSTRACT: Since the first synchronous communications satellite was launched in 1965, international communications satellites have entered the fifth generation. For domestic communications, satellites are officially being used in Canada, the USA, the USSR, Indonesia, and Japan, while 16 countries are leasing the international satellites for domestic communications. In 1976, the International Broadcasting Satellite Conference was held to determine 12GHz as the major frequency band for the television broadcasting satellite, etc. but to this day, the television broadcasting satellite system has not been officially put to use. This paper discusses the technical and economical problems of the 2 types of satellite systems in geographically large countries, such as Canada, the USA, and China. It is the author's opinion, following the analysis, that the establishment of a communications satellite system to take care of television broadcasting on the side is the technically and economically most reasonable way.

6248
CSO: 4009

END

END OF FICHE DATE FILMED

3/12/81